Current Opinion in Solid State and Materials Science 14 (2010) 69–74

Contents lists available at ScienceDirect

Current Opinion in Solid State and Materials Science

journal homepage: www.elsevier.com/locate/cossms

Nanoindentation-induced phase transformation in (1 1 0)-oriented Si single-crystals

Sheng-Rui Jian [a,*], Guo-Ju Chen [a], Jenh-Yih Juang [b]

[a] Department of Materials Science and Engineering, I-Shou University, Kaohsiung 840, Taiwan
[b] Department of Electrophysics, National Chiao Tung University, Hsinchu 300, Taiwan

ARTICLE INFO

Article history:
Received 28 July 2009
Accepted 26 November 2009

Keywords:
Si(1 1 0)
Nanoindentation
Focused ion beam
Cross-sectional transmission electron microscopy

ABSTRACT

Pressure-induced plastic deformation and phase transformations manifested as the discontinuities displayed in the loading and unloading segments of the load–displacement curves were investigated by performing the cyclic nanoindentation tests on the (1 1 0)-oriented Si single-crystal with a Berkovich diamond indenter. The resultant phases after indentation were examined by using the cross-sectional transmission electron microscopy (XTEM) technique. The behaviors of the discontinuities displayed on the loading and re-loading segments of the load–displacement curves are found to closely correlate to the formation of Si-II metallic phase, while those exhibiting on the unloading segments are relating to the formation of metastable phases of Si-III, Si-XII, and amorphous silicon as identified by TEM selected area diffraction (SAD) analyses. Results revealed that the primary indentation-induced deformation mechanism in Si is intimately depending on the detailed stress distributions, especially the reversible Si-II ↔ Si-XII/Si-III phase transformations might have further complicated the resultant phase distribution. In addition to the frequently observed stress-induced phase transformations and/or crack formations, evidence of dislocation slip bands was also observed in tests of Berkovich nanoindentation.

© 2009 Elsevier Ltd. All rights reserved.

1. Introduction

It is well known that silicon with cubic diamond structure (Si-I) when subjected to high-pressures will exhibit a series of crystal structure changes, usually irreversible, during both loading and unloading processes. Diamond anvil cell (DAC) studies have suggested that Si-I can transform into a metallic β-Sn phase (Si-II) under hydrostatic pressures of 11.2–12 GPa [1]. However, when the pressure is released, there is no evidence indicating direct transformation back to the original cubic diamond structure. Instead, Si-II transforms into various metastable phases depending on the details of load release conditions. For instance, it was observed that, with slow unloading in DAC, the Si-II first transforms into a rhombohedral structure, *r*8 (Si-XII), at 10–12 GPa, then proceed to exhibit a reversible transformation from Si-XII to the body-centered cubic structure, *bc*8 (Si-III), with further decrease in cell pressure, and eventually leading to a mixture of Si-III and Si-XII at ambient pressure [2]. These two structures, *bc*8 (Si-III) and *r*8 (Si-XII), retain distorted covalent-style tetrahedral bonding and are more densely packed than the cubic diamond structure. On the other hand, Zhao et al. [3] proposed that the Si-II would transform to a tetragonal phase (Si-IX) with rapid unloading from a DAC pressure of 14–15 GPa, albeit that such result has never been repeated by other groups. Yet another variant identified as the hexagonal diamond structure or Si-IV (wurtzite structure) [4] is observed when Si-III is heated. This phase is commonly regarded as an intermediate phase before the final recovery to Si-I.

While DAC experiments have provided rich information about the transformation mechanisms between various Si phases when under hydrostatic pressure as well as the associated mechanical characteristics of each phase, it is also anticipated that the transformation mechanisms between various Si phases and the pressures at which the transformations take place may change when non-hydrostatic stress is applied. In this respect, nanoindentation not only has proven to be a powerful technique in providing information on mechanical characteristics of the investigated materials but also being considered to be more relevant to realistic contact loading conditions encountered in various chip fabrication processes. In practice, the nanoindentation measurements are performed by measuring the displacement of the material as a function of the load applied to the tip of the indenter. Since, depending on the tip used, the distribution of the load can be very different, the manifesting physical properties and the deformation mechanisms involved may be drastically varied. As a result, although the results of nanoindentation contain much information concerning the prevailing deformation mechanisms at various stages, the interpretation of these data is by no means straightforward. Indeed, despite of the large body of indentation researches performed on Si recently [5–13], there are still some discrepancies between the obtained results. For instance, Mann et al. [11] pointed out that sharp indenter tip may result in small amount of Si-III and larger amount of amorphous Si (*a*-Si), while Bradby et al. [12,13] identified a thin layer of

* Corresponding author. Tel.: +886 7 6577711x3130; fax: +886 7 6578444.
E-mail address: srjian@gmail.com (S.-R. Jian).

1359-0286/$ - see front matter © 2009 Elsevier Ltd. All rights reserved.
doi:10.1016/j.cossms.2009.11.002

Si-XII with both sharp and spherical indenter tips. Jang et al. [8] further made systematic studies on the nanoindentation-induced phase transformations in Si and demonstrated the significant influences of loads, loading rate and indenter angle on the phase transformation behaviors. It is conceivable that with the large stresses, defect formation, cracking and piling-up generated in the vicinity of indenter, the responses of the system are inevitably becoming very complicated. Therefore, surface and subsurface phenomena need to be identified in a more direct manner, which unfortunately is not provided by the nanoindentation technique itself. To this respect, the focused ion beam (FIB) miller is now widely used for preparing the cross-sections of the locally deformed areas to direct reflect the detailed nanoindentation-induced mechanical responses for a range of materials [14]. In our case here, the cross-sectional observations can provide important information about the in-depth phase distribution and embedded defect features introduced by contact loading that were impossible to be observed with the plan-view samples.

From the practical point of view, since phase transformations significantly affect the electrical, optical and mechanical characteristics of the products, it is very important to have accesses in evaluating the materials subjected to the machining processes ubiquitously practiced in manufacturing Si substrates as well as the associated micro-electro-mechanical systems and microelectronics devices. In this paper, we will first give a brief account on the indentation-induced phase transformations in Si, especially on the mechanisms of how the Si-II phase transforms into the high-pressure phases of Si-XII/Si-III and/or *a*-Si during unloading, which has been an extensively debated issue recently. Then, the results on the deformation mechanisms of single-crystal (1 1 0)-Si under contact loading will be presented. In particular, the final structures of the indentation-induced transformation zone were analyzed using cross-sectional transmission electron microscopy (XTEM) techniques. The use of the Berkovich indenter not only will reflect the more realistic situations which might be encountered in real applications but also will result in much higher local pressure with similar load, and hence, will be helpful in clarifying the pressure-induced phase transformation issues. Furthermore, as indicated very recently by Gerbig et al. [10], the increased deviatoric loading for (1 1 0)-Si as compared with (0 0 1)-Si may facilitate plastic deformation processes leading to decreased transformation pressures. Thus, a timely confirmation on this with direct microstructural evidences should be of great interests.

2. Phase transformation in Si during unloading

Previously, a detailed account on the phase transformations in silicon under contact loading had been given by Domnich and Gogotsi [15]. In that, the phase transformation sequence of Si under contact loading and unloading has been rigorously indentified by the extensive combined studies of load–displacement measurements and Raman spectroscopy. Briefly, it was concluded that the pop-out during unloading is a consequence of Si-II → Si-XII transformation, which is believed to be accompanied by a sudden volume expansion resulting in the uplift of materials surrounding the indenter. Whereas the feature of an elbow appearing in the unloading curve is a result of material's expansion due to the slow amorphization of the metallic Si-II phase. In addition, it was also established that a pressure of $\sim$12 GPa is needed for the Si-I → Si-II transformation on (re)loading and 5–8 GPa for the Si-II → Si-XII transformation on unloading. For Si-III, the favorite pressure range is further reduced to 2–3 GPa [2]. However, as revealed by the direct microstructure evidences obtained from XTEM, the phase transformations during unloading are much more complicated than expected. For instance, Ge et al. [6] pointed out that there might be two possible transformation routes during the indentation of Si. The first is that, due to the extreme deformation introduced during indentation, direct amorphization of the Si-I occurred. The resultant a-Si can be retained in the transformation zone if the unloading is fast enough to quench the structure. If the unloading is slow the a-Si may transform into Si-III and Si-XII simultaneously, albeit this process has never been observed in high-pressure DAC experiments. Alternatively, the metallic Si-II phase is formed during loading provided the contact pressure exceeds 12–13 GPa which might be easily reached under a Berkovich indenter. The Si-II phase then transforms into Si-XII and finally into Si-III as the unloading process proceeds. In this scenario, however, owing to the inhomogeneity of stress distribution [16], especially the shear stresses, and various degrees defect concentrations can all produce different degree of bond breaking and lattice rotations, resulting in the formation of a mixture of Si-XII, Si-III, Si-I and a-Si within the same transformation zone, as revealed by their HRTEM observations. We note that within the framework of these two scenarios the correlations between the various features appearing on the load–displacement curves became arguable.

On the other hand, recent study on the formation and growth of indentation-induced high-pressure phases made by Ruffell et al. [17] has revealed that the transformation of Si-II to high-pressure phases on unloading can be explained primarily by a nucleation and growth mechanism [8,13]. By comparing the phase distributions quenched from various stages on the unloading curves, Ruffell et al. concluded that the seed nuclei of Si-III and Si-XII form during very early stages of unloading and substantial volume of both phases occurs only after the pop-out event at about 50% of the maximum load. In contrast, high-pressure phases form more readily and substantially in *a*-Si matrix without an observable pop-out event with rapid unloading. In other words, it appears that in the nano-indentation experiments the transformation between various phases of Si is not necessary following the pressure sequences established previously by the hydrostatic DAC experiments. Rather, it is more relevant to the detailed stress distribution, phases existent, and defect microstructures prior to uploading. In fact, similar conclusions were reached by Zarudi et al. [18,19]. Nevertheless, the issues of whether the new phases are emerging from nucleation and growth mechanism or activated by deformation-induced lattice rotation remain a matter of interest. One expects that in the former the dislocation density within the transformation zone should be much less than that in the latter, since the lattice rotation will generate more dislocations [6]. Furthermore, as mentioned above, the stress distribution induced by the Berkovich indenter in (1 1 0)-Si substrates can be also very different from that obtained mostly from the spherical indenter and on (0 0 1)-Si substrates.

3. Experimental details

Single crystalline (1 1 0)-Si wafers with light boron doping (1×10^{15} atoms/cm^3) were used in the experiment. The wafers were first ultrasonically cleaned for 20 min in acetone, then dipped into 5% HF aqueous solution for 30 min to remove the oxide layers, and followed by a thorough rinse in de-ionized water. Nanoindentation tests were performed on a MTS NanoXP® (MTS Cooperation, Nano Instruments Innovation Center, TN, USA) equipped with a three-sided pyramidal Berkovich diamond indenter. The indenter tip has a nominal radius of about 50 nm with the pyramidal faces forming an angle of 65.3° with the vertical axis. Cyclic nanoindentation measurements were performed by the following sequences. Firstly, the indenter was loaded to some chosen load and then unloaded by 90% of the previous load to complete the first cycle. It was then reloaded to a larger chosen load and unloaded by 90% for the second cycle. Fig. 1(a) displays the typical load–displacement results for the cyclic indentation test repeated for four cycles

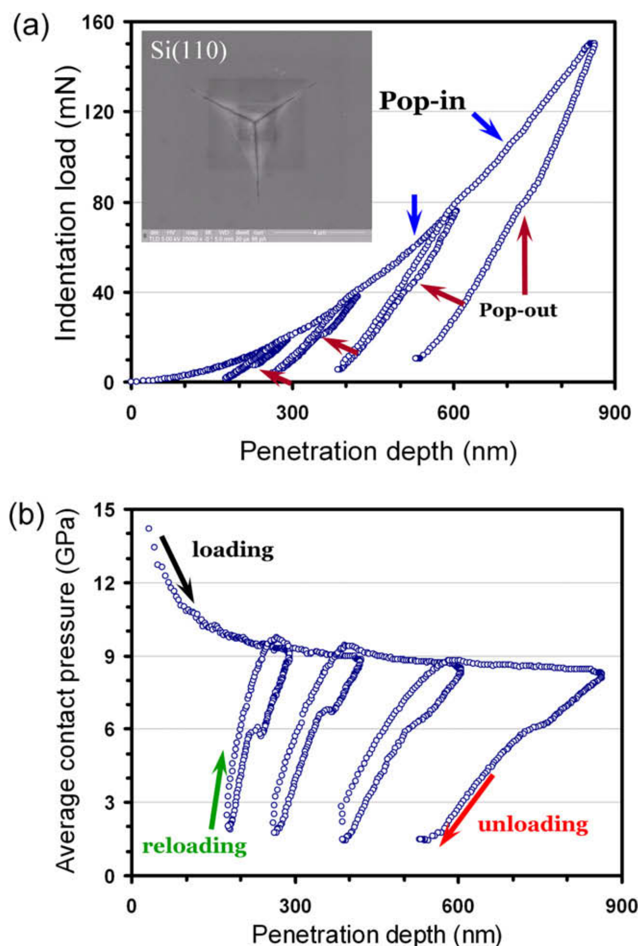

Fig. 1. (a) Load–displacement data for single-crystal Si(1 1 0) obtained during nanoindentation with a Berkovich indenter showing the multiple "pop-in" and "pop-out" events during loading and unloading, respectively. The inset shows a SEM micrograph of an indent made at an applied load of 150 mN. Notice the crack formation along the pyramidal edge directions. (b) Average contact pressure vs. penetration depth curves of cyclic nanoindentation on Si(1 0 0).

to finally reach at an indentation load of 150 mN. It is noted that, in each cycle, the indenter was hold for 5 s at 10% of its previous maximum load for thermal drift correction and for assuring that complete unloading was achieved. The thermal drift was kept below ±0.05 nm/s for all indentations considered in this study. The same loading/unloading rate of 1 mN/s was used.

Indents are cross sectioned using a FEI Nova 220 Dual-Beam workstation – FIB/SEM system to examine subsurface deformed microstructures, as described in details previously [20–22]. Prior to ion milling, a thin layer of Pt was deposited to protect the indents from ion-beam damage. Conventional TEM studies were carried out in a JEOL-2010 TEM operating at 200 kV.

4. Results and discussion

The load–displacement curve shown in Fig. 1(a) displays the typical Berkovich indentation behavior carried out on the Si(1 1 0) single-crystals with a maximum indentation load of 150 mN. In general, the indentation curves reveal much information, especially for silicon with rich phase transformations involved. As summarized by Gerbig et al. [10], the loading curve usually contains two segments: (i) the slope change associated to the primary phase transformation and, (ii) the plateau-like discontinuities (so-called "pop-in" events) associated to the plastic flow initiated in ductile Si-II phase. On the other hand, the unloading curve, depending on the operation conditions, can have as many as six segments: namely elastic behavior, plastic behavior, elbow, pop-out, kink pop-out, and elbow followed by pop-out. Among them, the elbow feature characterized by the gradual change of slope (dP/dh, with P being the load and h being the indentation depth, respectively) is attributed to associate with the material expansion during a slow amorphization of Si-II, while the pop-out characterized by a constant dP/dh is primarily due to the Si-II → Si-XII/Si-III transformation induced material expansion underneath the indenter.

As can be clearly seen, Fig. 1(a) apparently reproduces many features corresponding to different phase transformations. For instance, the continuous slope change during loading indicates the pressure-induced phase transformation is, in fact, occurring even at relatively low loadings in the present case. Moreover, as indicated by the arrows depicted as "pop-ins", there are some plastic flow events simultaneously prevailing in the system after some of the materials underneath the indenter tip has transformed to more deformable phase of Si-II. It is noted that the "pop-in" events have also been alternatively interpreted by attributing to the large volume change (∼22%) associated with the onset of Si-I → Si-II phase transformation, which is also expected to result in very different microstructure as compared to that described above [5,12,13,23]. Indeed, it has been argued [12] that at higher loads the initiation of slip, which primarily takes place on the {1 1 1} planes of the Si-I phase, may be terminated when a catastrophic pop-in (Si-I → Si-II) phase transformation occurs. In order to further explore this issue, we re-plot the indentation load shown in Fig. 1(a) with average contact pressure (Fig. 1(b)). The average contact pressure originally rapidly decreases during the first loading cycle with the penetration displacement then quickly reaches a more or less constant value of about 9 GPa. This behavior is consistent with those observed by Gototsi et al. [24] in (0 0 1)-Si, albeit the "saturated" average pressure value is about 3–4 GPa lower. It is also evident that during the first cycle the pop-in (the discontinuity on the upper-left corner) occurs at an average pressure of about 13 GPa, which is consistent with the transformation pressure of Si-I → Si-II (11.2–12 GPa) [1]. It is also noted that there are additional pop-ins occurring at an average contact pressure of about 7 GPa on all of the subsequent re-loading segments. Since it is apparently well below the threshold pressure of Si-I → Si-II, it might be resulting from different origins. However, whether these are due to other phase transformation-induced volume change or are related to plastic flow phenomena will need further discussions. The fact, that the pop-ins (discontinuities on the re-loading curves) and the pop-outs or elbows on the unloading segments are occurring at close range of contact pressures (6–7 GPa) suggests that these events are likely relevant to the reversible Si-XII/Si-III ↔ Si-II transformations, which has been found to occurring around 8 GPa in (0 0 1)-Si [24]. As indicated by Gerbig et al. [10], the deviatoric stress distribution, especially the shear stress, resulting from the Berkovich indentation would tend to lower the contact pressures at which the phase transformations take place in (1 1 0)-Si and (1 1 1)-Si than in (0 0 1)-Si. Alternatively, it is immediately suggestive from the scanning electron microscope (SEM) image displayed in the insert of Fig. 1(a) that the major subsequent pop-in occurs during the indentation loading curve might be associated with the cracking events along the corner of residual indentation [25]. However, as pointed out by Morris et al. [25], the fracture at the indentation site is not a sufficient condition for changing the unloading behavior and probably will not significantly alter the general features of phase transformations being discussed here. It is thus very interesting to investigate directly from the microstructure analysis to clarify whether the pop-ins are relating to the Si-I → Si-II phase transition or it is simply a manifestation of the sudden extrusion of highly plastic transformed materials from under-

neath the indenter, or even just being due to the initiation of cracks. Furthermore, it is also interesting to know whether or not the nanoindentation-induced generation and propagation of dislocations observed in III–V semiconductors [20–22] occurring in this system, as well.

Before getting into the microstructure analysis, the marked features seen in unloading segments of the load–displacement curve ought to be discussed in some details. As seen in Fig. 1, in addition to the issues of the pop-ins and the average contact pressure values (Fig. 1(b)) discussed above, in Fig. 1(a) the pop-out feature with $dP/dh \sim 0$ characterizing the Si-II → Si-XII phase transformation appears to happening only at lower loadings, whereas, at higher loadings, the pop-out features are primarily characterized by a finite dP/dh, implying an amorphization dominating process. In general, this agrees with the results reported in previous studies [26–28]. In that, upon unloading, the formation of mixture phases of Si-III and Si-XII is evidenced by pop-out event and the phase characterizations carried out by using micro-Raman spectroscopy [15,27] and TEM [12,18,19] within the residual indents. Thus, these phases and possibly the amorphous regions should the major residual phases expected in the following XTEM analyses.

A XTEM bright-field image, demonstrating the resultant morphology and microstructure of the transformation zone after subjected to an indentation load of 150 mN is shown in Fig. 2(a). The insert to the main panel shows the selected area diffraction (SAD) indicating the complex crystalline phases existing and possibly amorphous characteristics of the resultant material inside the deformed zone. The XTEM image displayed in the main panel of Fig. 2(a) shows that the transformation zone has a nearly pyramidal shape with a maximum penetration depth of ~600 nm. The slip bands running along the direction inclining at an angle of ~45° with respect to the indentation direction are also evident in Fig. 2(a). Since the substrate is of (1 1 0) orientation, such slip bands are parallel to the {1 1 1} planes. It is noted that the slip bands, similar to those reported by Haq and Munroe [23] are activated in the region outside the transformation zone and are distributing rather asymmetrically.

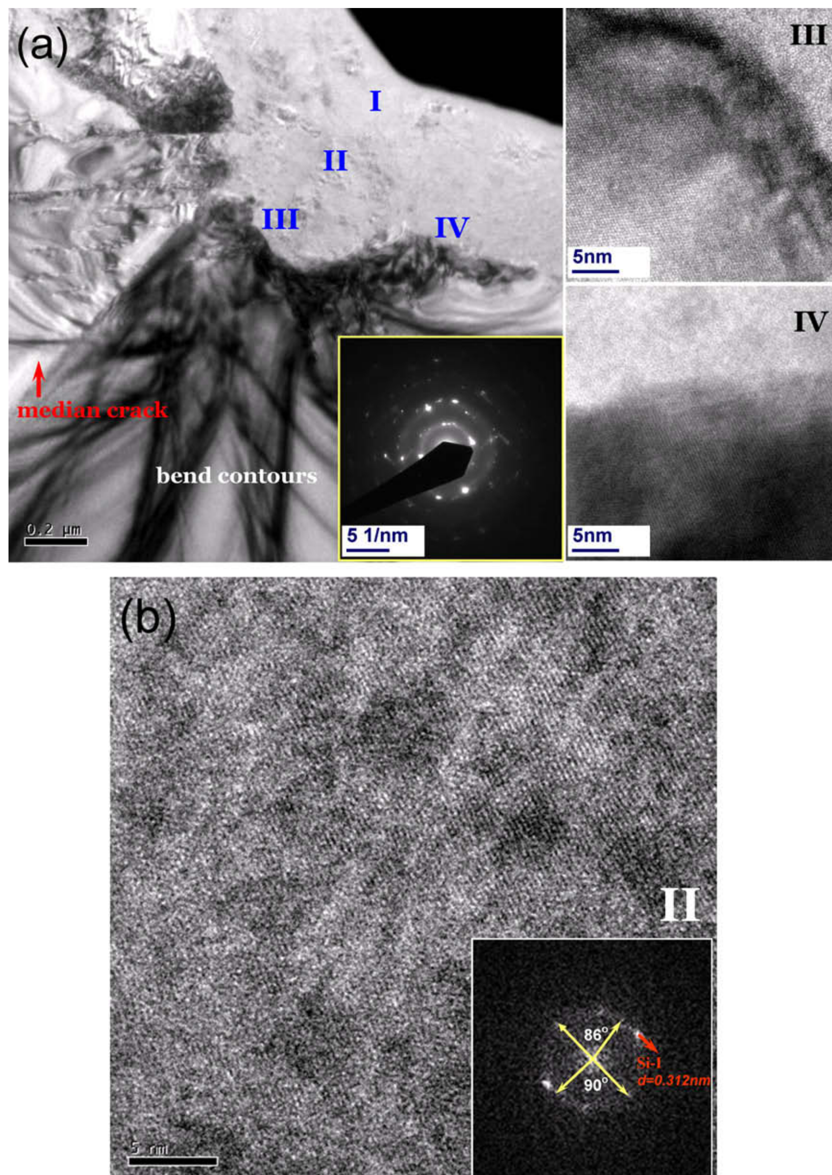

Fig. 2. (a) The bright-field XTEM image in the vicinity immediately under the Berkovich indent applied on single-crystal Si(1 1 0) with an indentation load of 150 mN. A residual indentation of ~150 nm deep is evident on Si surface upon which the indenter impressed, indicating a significantly plastic deformation; insert: SAD of transformed zone II is shown. Right hand side: HRTEM images of the transformed zones III and IV. (b) Magnified HRTEM image obtained from the transformed zone II and, insert: the corresponding FFT-simulated diffraction pattern.

It appears that the slip bands are concentrating near the tip edge while directly beneath the tip the dense contour in the XTEM image suggest severe deformation. Also, unlike that observed in (1 1 1)-Si by Haq and Munroe [23] where slip was found on {3 1 1} planes, we only observe the {1 1 1} slip bands. The asymmetric distribution of crystalline defects is believed to originate from the stress distribution caused by the Berkovich indenter. Indeed, Zarudi et al. [16] has simulated the stress distribution and found that the highest hydrostatic stress in the substrate under the Berkovich indenter is right beneath the tip, while for the octahedral (shear) stress the highest stress is distributed adjacent to the edges near the tip. The slip bands active region seen on the upper left hand side of Fig. 2(a), thus are likely to result from highly concentrated shear stress existent in that region. We note that both the present results and that reported in Ref. [23] are consistent with the predicted ones. Furthermore, it is likely that the median crack is initiated at the intersection of the slip bands and the boundary between the primary deformation zone and the untransformed Si-I region due to the significant pile-up of slip bands. The fact that there is also a sharp boundary between the shear stress driving slip region and the marked dislocation activity phenomena observed immediately beneath the transformation zone could also reflect the different natures of the dominant stress in the respective regions. As the slip bands intersect at the boundary of the two regions, it can act as barrier obstructing further dislocation gliding leading to the rapid stress accumulation and subsequent formation of median crack [23]. It is noted that similar observations were made in nanoscratch experiments performed on Si, as well [19]. It is interesting to note that in the present case the median crack is formed at a location about 1 μm below the bottom of the transformation zone and somewhat away from the line extending from the tip center, which is very different from that obtained from the (0 0 1)-Si substrates by either the spherical indenter [12] or the Berkovich indenter. In that the median cracks were evidently observed right at the tip beneath the transformation zone. The formation of the median crack beneath the slip band apex indicates that the rapid accumulation of induced stress in this local region. As a result, the differences in the median crack formation observed in substrates with different crystallographic orientations might be originated from the detailed distribution of contact pressure and the active dislocation slip systems driven by these stresses. Finally, it is also noted that material from the transformation zone appears to have extruded into the regions with marked dislocation slip activities resulting in the rather irregular boundary between the transformation zone and the untransformed regions. It is consistent with the "bumps" exhibited near the maximum contact pressure on the reloading cycles seen in Fig. 1(b), which has been indentified as the signature of the significant plastic flow prevailing in the ductile metallic Si-II phase under contact loading [24,29,30]. In other words, the current results indicate that during the later load–unload cycles, the reversible transformations between Si-II and the high-pressure Si-XII and Si-III are probably the primary process accompanied by significant dislocation activities.

Next, we turn to discuss the detailed microstructures within the transformation zone. The observed amorphous phase in the upper part of the transformed zone (region I) agrees with the previous XTEM studies by Bradby et al. [12,13] who reported that, in relatively large spherical indentations on Si, evidence of amorphous silicon can be found at the centre of indentation near the material surface. However, any surface asperities on the indenter tip could generate large shear stresses close to the surface and, therefore, generate the amorphous silicon in this local region. A reasonable explanation for such phase distribution is that the surface layer is less constrained than the deeper region and, thus has no enough time to rearrange into another crystalline phase from the high-pressure phase Si-II during pressure release. We note that this is also consistent with the results reported by Zarudi et al. [16] wherein, for Berkovich indenter-induced transformation, near the surface of the transformation zone is dominated by *a*-Si and in the deeper region of the zone mixture of Si-XII and Si-III are evidently identified, whereas, for spherical indenter, the Si-XII and Si-III are found only in the center of the transformation zone with all the surrounding regions being *a*-Si.

High resolution TEM (HRTEM) images of the transformation zone locating near the crack apex and the pyramidal side area, such as the regions III and IV indicated in Fig. 2(a), are displayed in the right hand side pictures, respectively. It is noted that near the proximity region toward region II appears to be irregular along the boundary. On the other hand, in region IV, mostly amorphous phase is observed. In the present case, since it takes four cycles to reach to the 150 mN loading condition for the sample under XTEM examination, the structures, as discussed above, might have experienced several cycles of Si-II ↔ Si-XII/Si-III transformations. Indeed, as revealed in Fig. 2(b), the seemingly amorphous region II indicated in Fig. 2(a) actually is composed of many nanocrystals of high-pressure phases embedded in the amorphous matrix (see below). The detailed phases and their distributions within the transformation zone in the current study, thus, may not directly comparable to those revealed in the previous studies [16,17,23,30], in that, most results were obtained by single-cycle indentation test. Nevertheless, the observations consistently indicate that boundary structure and the detailed stress distribution are playing the primary role in determining the resultant phases and their distribution within the transformation zone in the contact-induced phase transformation of Si. Being the source of defects and the stress concentrator, the boundary between the transformation zone and the untransformed bulk can act as the primary nucleation sites of the new phases or as the sites for initiating the amorphous phase transformation due to the accumulated stress near the slip bands intersects. Moreover, it is likely that the energetic crack tip progresses straight down into the crystal immediately after its formation could also release significant amount of energy along the propagation and influences the structure of the adjacent material. This may also explain why markedly different microstructure are present in region III and region IV, despite both are about the same position from the indenter tip.

Complementary to the SAD technique, HR-image observations provide additional structural information to reveal lattice structures of different phases formed during nanoindentation and are of indispensable importance in helping understand the prevailing mechanisms involved in phase transformations, especially for phases such as Si-III and Si-XII which are structurally similar. For instance, in the apparently unsmooth region II indicated in Fig. 2(a), the HR image (Fig. 2(b)) evidently displays features showing that the ordered crystalline lattice was broken into nano-sized grains with different crystalline orientations. This indicates that in this region the lattice are significantly distorted when subjected to Berkovich nanoindentation. With the aid of the fast Fourier transformation (FFT) method, the diffraction pattern of HRTEM image of region II is simulated, as shown in the inset of Fig. 2(b). By measuring the interplanar angles from the simulated FFT diffraction pattern, the structural characteristics of Si-III and Si-XII in the centre part of the transformed zone are evidently identified. Namely, the results indicate that the diffraction pattern is in fact an overlapped result of two phases; the one with 90° interplanar angle is from the cubic Si-III, whereas the phase with 86° interplanar angle is Si-XII. The results thus imply that the transformation from Si-II to Si-XII/Si-III may have occurred simultaneously by random nucleation and growth during unloading. However, depending on the stress distribution and the detailed unloading conditions, the more ordered crystalline regions can also nucleate near the boundary between the transformation zone and untransformed bulk, as has been pointed out by Ruffel et al. [17] and others [16,23,30].

5. Conclusions

In summary, we investigated the contact-induced phase transformation in Si(1 1 0) single-crystals by combining techniques of Berkovich nanoindentation, FIB and TEM observations. The load–displacement curves obtained from the Berkovich indentation test displayed distinct features of stress-induced and afterward unloading phase transformations as previously anticipated, albeit at lower loads than that observed in Si(0 0 1) crystals. The structural analyses carried out in the residual indentation regions immediately beneath the indenter tip confirmed the presence of metastable phases in the course Berkovich nanoindentation-induced phase transformations in Si(1 1 0) single-crystals. Median cracking and dislocation generation are also observed around the transformation zone. As evident from XTEM results, two structurally similar metastable phases, Si-III and Si-XII, and amorphous phase, have been distinguished by electron diffraction and their spatial distribution within residual Berkovich nanoindentation were examined. The results from this study should be helpful to clarify the deformation mechanisms and the subsurface damage mechanisms of Si when subjected to nanometer-scale mechanical contacts.

Acknowledgements

This work was partially supported by the National Science Council of Taiwan and I-Shou University, under Grant Nos.: NSC 97-2112-M-214-002-MY2, ISU97-07-01-04 and ISU 97-S-02. JYJ is supported in part by the National Science Council of Taiwan and the MOE-ATP program operated at NCTU.

References

[1] Mujica A, Rubio A, Muñoz A, Needs RJ. Rev Mod Phys 2003;75:863.
[2] Grain J, Ackland GJ, Maclean JR, Piltz RO, Hatton PD, Pawley DS. Phys Rev B 1994;50:13043.
[3] Zhao XS, Buehler F, Sites JR, Spain IL. Solid State Commun 1986;59:678.
[4] Besson JM, Mokhtari EH, Gonzalez J, Weill G. Phys Rev Lett 1987;59:473.
[5] Zarudi I, Zou J, Zhang LC. Appl Phys Lett 2003;82:874.
[6] Ge D, Domnich V, Gogotsi Y. J Appl Phys 2003;93:2418.
[7] Ge D, Domnich V, Gogotsi Y. J Appl Phys 2004;95:2725.
[8] Jang J, Lance MJ, Wen S, Tsui TY, Pharr GM. Acta Mater 2005;53:1759.
[9] Lin YH, Chen TC, Yang PF, Jian SR, Lai YS. Appl Surf Sci 2007;254:1415.
[10] Gerbig YB, Stranick SJ, Morris DJ, Vaudin MD, Cook RF, J Mater Res 2009;24:1172 [and references therein].
[11] Mann AB, van Heerden D, Pethica JB, Bowes P, Weihs TP. Philos Mag 2002;A82:1921.
[12] Bradby JE, Williams JS, Leung JW, Swain MV, Munroe P. Appl Phys Lett 2000;77:3749.
[13] Bradby JE, Williams JS, Leung JW, Swain MV, Munroe P. J Mater Res 2001;16:1500.
[14] Wasmer K, Ballif C, Gassilloud R, Pouvreau C, Rabe R, Michler J, et al. Adv Eng Mater 2005;7:309.
[15] Domnich V, Gogotsi Y. Rev Adv Mater 2002;3:1.
[16] Zarudi I, Zhang LC, Cheong WCD, Yu TX. Acta Mater 2005;53:4795.
[17] Ruffell S, Bradby JE, Williams JS, Munroe P. J Appl Phys 2007;102:063521.
[18] Zarudi I, Zhang LC, Zou J, Vodenitcharova T. J Mater Res 2004;19:332.
[19] Zarudi I, Nguyen T, Zhang LC. Appl Phys Lett 2005;86:011922.
[20] Chien CH, Jian SR, Wang CT, Juang JY, Huang JC, Lai YS. J Phys D: Appl Phys 2007;40:3985.
[21] Jian SR, Juang JY, Lai YS. J Appl Phys 2008;103:033503.
[22] Jian SR. Appl Surf Sci 2008;254:6749.
[23] Haq AJ, Munroe PR. J Mater Res 2009;24:1967.
[24] Gotosi YG, Domnich V, Dub SN, Kailer A, Nickel KG. J Mater Res 2000;15:871.
[25] Morris DJ, Myers SB, Cook RF. J Mater Res 2004;19:165.
[26] Domnich V, Gogotsi Y, Dub S. Appl Phys Lett 2000;76:2214.
[27] Yan XQ, Huang XM, Uda S, Chen MW. Appl Phys Lett 2005;87:191911.
[28] Jang J, Pharr GM. Acta Mater 2008;56:4458.
[29] Morris JC, Callahan DL. J Mater Res 1994;9:2907.
[30] Kailer A, Gogotsi YG, Nickel KG. J Appl Phys 1997;81:3057.